A theoretical study on the aromaticity of benzene and related derivatives incorporating a C–CC–C fragment

ARTICLE *in* TETRAHEDRON · SEPTEMBER 2013

Impact Factor: 2.64 · DOI: 10.1016/j.tet.2013.06.072

Tetrahedron 69 (2013) 7333–7344

Contents lists available at SciVerse ScienceDirect

Tetrahedron

journal homepage: www.elsevier.com/locate/tet

A theoretical study on the aromaticity of benzene and related derivatives incorporating a C–C≡C–C fragment

Goar Sánchez-Sanz [a,*], Cristina Trujillo [a], Isabel Rozas [b], José Elguero [c]

[a] Institute of Organic Chemistry and Biochemistry, Gilead Sciences Research Center & IOCB, Academy of Sciences of the Czech Republic, Flemingovo nám. 2, 166 10 Praha 6, Czech Republic
[b] School of Chemistry, Trinity Biomedical Sciences Institute, Trinity College Dublin, 152-160 Pearse St., Dublin 2, Ireland
[c] Instituto de Química Médica, CSIC, Juan de la Cierva, 3, E-28006 Madrid, Spain

ARTICLE INFO

Article history:
Received 18 May 2013
Received in revised form 18 June 2013
Accepted 20 June 2013
Available online 29 June 2013

Dedicated to Professor Ibon Alkorta on the occasion of his 50th anniversary

Keywords:
Dehydroannulenes
Aromaticity
NICS
Chemical shifts
Benzene

ABSTRACT

Continuing with our interest in aromaticity, we have studied the influence that replacement of formal C–C single bonds by C–C≡C–C fragments, in a series of mono- (cyclobutadiene, benzene, and cyclooctatetraene) and fused-carbocycles (naphthalene and azulene), has in their properties, focusing mostly on NMR and aromaticity. We have analyzed the effect of such substitution not only in the aromaticity of the different structures, but also in the influence of low and high spin states by means of NICS values over the rings and 3D NICS isosurfaces. We have found that, in most of the cases, the substitution induces a loss of aromaticity in singlet states (both restricted and unrestricted) that can be recovered when triplet states are taken into account.

1. Introduction

Research on aromaticity has produced many different studies. Thus, from an structural point of view and starting from the paradigmatic benzene, the classical two-dimensional aromatic structure of hydrocarbons can be extended in different ways, for example, by: (i) increasing the number of benzene rings, i.e., from naphthalene to graphene;[1,2] (ii) changing the size of the ring, i.e., from cyclopropene to annulenes;[3] (iii) adding charges like in the tropylium cation;[4] or (iv) replacing double bonds by triple bonds, i.e., from benzyne to dehydroannulenes.[4–7] Moreover, 2D carbon structures, such as graphyne[8] or graphydine,[9,10] have attracted the attention of the scientific community as nanomaterials for their electronic properties. Furthermore, another interesting aspect related to aromaticity that has been previously studied is the aromaticity/antiaromaticity inversion observed between the ground and the excited states of cyclooctatetraene.[11–13]

Continuing with our interest in aromaticity,[13–16] and considering the mentioned studies on aromaticity extension and properties, in the present study we are approaching a different question: what happens to the aromatic properties of a ring when a C–C≡C–C fragment replaces a formal single C–C bond in one of the Kekulé's structures? In principle, the most obvious consequences will be that, as the length between the unchanged C atoms increases, the ring-strain effects would be modified[17] and that two new π electrons are added. This last fact will change an aromatic compound into an antiaromatic one, for each replacement, and the opposite for an antiaromatic system. Our approach has a topological consequence (how to generate new conjugated rings) and a structural one (how to describe the resulting rings).

The 15 structures that will be examined in the present work are represented in Fig. 1. Apart from the five parent compounds (**1**, **3**, **5**, **10**, and **14**), only **9** is a well-known structure.[14,18,19] Compound **6**, which was considered the dehydroannulene of cyclooctatetreene (compound **3** or COT), has been experimentally isolated[20] and theoretically studied.[18]

Several dehydroannulenes derived from COT were theoretically studied by Yavari and Norouzi-Arasi but none coincides with those of Fig. 1.[21] COT itself has been the subject of three relevant articles; thus, in 2008 Karadakov[22] studied the aromaticity and antiaromaticity of the low-lying electronic sates of COT and, more recently, Manz et al.[23] explored the topology of its symmetric

* Corresponding author. E-mail addresses: goar@iqm.csic.es, hidroargiros@gmail.com (G. Sánchez-Sanz).

0040-4020/$ – see front matter © 2013 Elsevier Ltd. All rights reserved.
http://dx.doi.org/10.1016/j.tet.2013.06.072

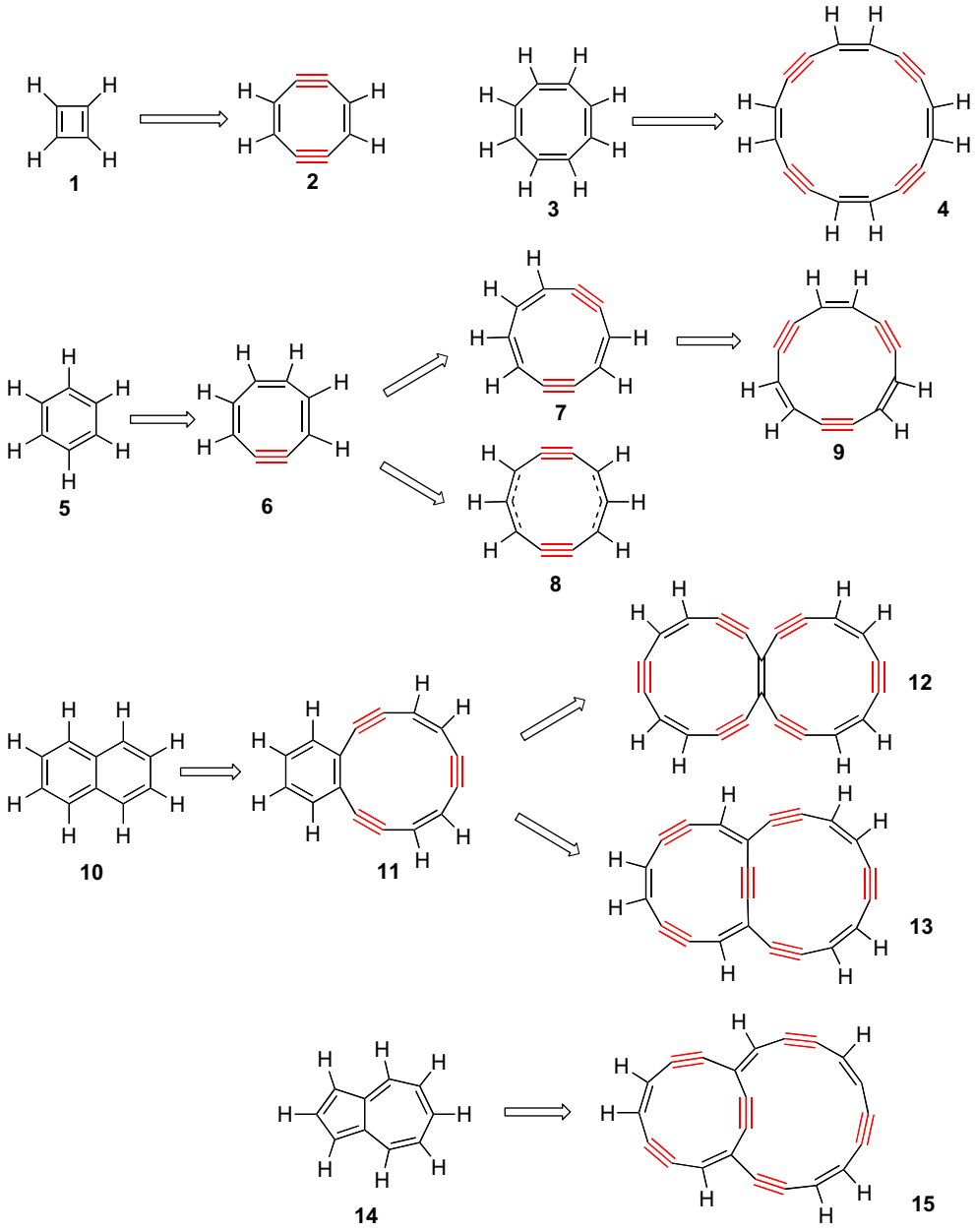

Fig. 1. Different compounds studied in the present work.

quadruple minimum potential energy surface (PES). Additionally, Schleyer et al. explained why COT is highly stabilized.[24] Recently, a study of the antiaromatic planar cyclooctatetraene has pointed out the properties of this compound as semiconductor.[7] In Table 1, we have summarized the information related to these compounds, i.e., their molecular formula, the number of substitutions, and their systematic name (only for compound **3** we will use the well-accepted COT abbreviation).

2. Computational details

The geometry of the systems has been optimized at the B3LYP[25,26]/6-311++G(d,p)[27] computational level. Frequency calculations have been carried out to confirm that the structures obtained correspond to energetic minima or true transition states (TS). Previous studies[13] suggest than in these compounds unrestricted wave function solutions may become more stable than closed shell ones, therefore, singlet closed shell (S), unrestricted open shell (U), and triplet states (T) have been studied. In addition, the stability of the wave function at the HF level has been checked to confirm that the structures obtained do not show any electronic instability.

NICS(0), (1) and (2), values[28] were calculated using the GIAO method[29,30] on the B3LYP/6-311++G(d,p) geometries over the ring center at 0, 1, and 2 Å respectively. To obtain the spatial distribution of the NICS, its values have been calculated on a 3D cubic grid of different sizes (8, 12, 14, and 16 Å) following the procedure described in Refs. 13 and 15. The points in the grid are located at 0.2 Å one from another in the three spatial directions. The result is a cube of *n* NICS values (depending on the cube size, up to 531,441 values), which in the next step were represented over the 0.001 a.u. electron density isosurface using the WFA program.[31] All the calculations have been carried out with the Gaussian09 computational package.[32]

Table 1
Carbocycles obtained by replacement of a C–C bond by a C–C≡C–C fragment, the number of H atoms does not change but the number of C atoms changes from 2*n* to 4*n* (*n*, number of replacements)

Comp.	Formula	*n*	Name
1	C_4H_4	0	Cyclobutadiene
2	C_8H_4	2	Cycloocta-1,5-diene-3,7-diyne
3	C_8H_8	0	Cyclooctatetraene (COT)
4	$C_{16}H_8$	4	Cyclohexadeca-1,5,9,13-tetraen-3,7,11,15-tetrayne
5	C_6H_6	0	Benzene
6	C_8H_6	1	Cycloocta-1,3,5-trien-7-yne
7	$C_{10}H_6$	2	Cyclodeca-1,3,7-trien-5,9-diyne
8	$C_{10}H_6$	2	Cyclodeca-2,7-dien-4,9-diyn-6-ylium-1-ide
9	$C_{12}H_6$	3	Cyclododeca-1,5,9-trien-3,7,11-triyne or 1,5,9-tridehydro[12]annulene
10	$C_{10}H_8$	0	Naphthalene
11	$C_{16}H_8$	3	5,6,9,10,13,14-Tridehydrobenzo[12]annulene
12	$C_{22}H_8$	6	1,2,5,6,9,10,11,12,15,16,19,20-Hexadehydrocyclododeca[12]annulene
13	$C_{22}H_8$	6	Bicyclo[10.8.2]docosa-1(20),4,8,12,16-pentaen-2,6,10,14,18,21-hexayne
14	$C_{10}H_8$	0	Azulene
15	$C_{22}H_8$	6	Bicyclo[11.7.2]docosa-1,5,9,13,17-pentaen-3,7,11,15,19,21-hexayne

The natural bond orbital (NBO) method[33] has been employed to evaluate the Wiberg bond indexes (WI) within the natural resonance theory (NRT).[34,35]

In order to evaluate the π-electron delocalization on the compounds studied, and thus, the aromaticity, the harmonic oscillator model of aromaticity (HOMA) has been used.[36,37]

3. Results and discussion

The different compounds will be named using the numbers presented in Fig. 1 and adding an S, TS, T or U to design singlet closed shell, singlet transition states, triplet states and unrestricted open shell states, respectively. Since all TSs correspond to singlet states this term will be avoided in the discussion.

3.1. Energy and structure

The optimized structures of all the compounds studied and their total energies can be found in Supplementary data (Table S1 and Fig. S1).

3.1.1. Structural results. In Table 2, the bond distances for all the compounds studied have been summarized. In the case of the planar compound **1**, substitution of two C–C bonds by two C–C≡C–C fragments, leads to an eight-membered ring with boat-like structure (compound **2**). The starting planar configuration for **2** was optimized and the resulting geometry (**2TS**) was a transition state. Once the optimization is achieved, following the gradient vector corresponding to the imaginary frequency, the boat-like structure was found.

Table 2
Bond distances (Å) at B3LYP/6-311++G(d,p) geometries for the compounds studied

Compound	*d*(C–C)	*d*(C=C)	*d*(C≡C)	Compound	*d*(C–C)	*d*(C=C)	*d*(C≡C)
1S	1.577	1.333	—	**9S**	1.326	1.475	1.261
2S	1.480	1.384	1.380	**9U**	1.416	1.356	1.212
2TS	1.472	1.396	1.384	**9T**	1.369	1.410	1.235
2T	1.456	1.437	1.454	**10S**	1.418	1.374[b]	—
3S	1.472	1.34	—	**11S**	1.410[a]	1.386[a]	1.212[a]
3TS	1.409	1.408	—	**12S**	1.363[a]	1.436[a]	1.236[a]
3T	1.403	1.403	—	**12U**	1.406[a]	1.376[a]	1.217[a]
4S	1.409	1.355	1.214	**12T**	1.390[a]	1.397[a]	1.223[a]
4TS	1.408	1.355	1.214	**13S**	1.359[a]	1.441[a]	1.240[a]
4T	1.369	1.399	1.234	**13U**	1.413[a]	1.363[a]	1.213[a]
5S	1.395	1.395	—	**13T**	1.386[a]	1.400[a]	1.226[a]
6S	1.460[a]	1.349[a]	1.208	**14S**	1.407[a]	1.407[a]	—
7S	1.374[a]	1.394[a]	1.230	**15S**	1.408[a]	1.369[a]	1.216[a]
8S	1.366	1.401	1.233				

[a] Average values.
[b] Central bond not included.

The same procedure was followed for compound **3** (COT) where four substitutions were performed simultaneously, leading to compound **4**. As in previous studies, where the different structures of COT had been analyzed, in the present work we have calculated the boat-like singlet ground state (**4S**), transition state (**4TS**), and triplet state (**4T**). All of them show similar structures to those of COT (**3S**, **3TS**, and **3T**, respectively).

In the case of benzene (**5**), a different approach was followed. The replacement of *n*C–C bonds by *n*C–C≡C–C fragments was performed sequentially (*n*=1, 2, and 3) to study the effect of *n* on the aromaticity.

For naphthalene (**10**), only one C–C bond has been replaced, yielding compound **11**; when the replacement was performed in both rings, compounds **12** and **13** resulted. Finally, for azulene (**14**), all the C–C bonds have been replaced simultaneously, yielding compound **15**.

The detailed changes observed in the structural properties of the double bonds after the conversion from the parent compound to the substituted one can be found in Supplementary data. In compound **1**, the C=C bond distance is 1.333 Å, while in derivatives **2S**, **2TS**, and **2T** it elongates to 1.384, 1.396, and 1.437 Å, respectively. In compound **2** the interconversion between the boat-like **2S** and its transition state **2TS**, slightly modifies the C bonds, the largest variation being observed in the C=C, with an elongation of 0.012 Å. When the triplet is taken into account (**2T**), the geometry differs from that of the singlet, showing an increment in the C=C and C≡C bonds (0.053 and 0.074 Å respectively), while the C–C bonds decrease by 0.024 Å. In addition, the C=C Wiberg index (WI)[34,35] for compound **1** (Fig. S1) slightly decrease from 2 to 1.6 in **2S** and **2TS**, and down to 1.4 in **2T**. The reduction of the WI from 1.6 (**2S**, **2TS**) to 1.4 (**2T**) suggests a more uniform electron distribution. Furthermore, the substitution on the boat-like (**2S**) and the planar (**2TS**) seems to have similar effects on the distances (see the next sections) and on the aromaticity.

The same effect was found in the **3TS** singlet (elongation of C=C and shortening of C–C bonds, with WI of 1.9 and 1.1, respectively) and in the **3T** (uniform distribution of bonds with a WI=1.4) with respect to the ground state **3S**. When the four-fold substitution is carried out, comparing **3S** and **4S**, it can be observed that C=C bonds are slightly longer in the latter. Comparison between **4S**, its transition state (**4TS**) and the triplet one (**4T**) shows that the structural changes observed are similar to those found for compound **2**. While **4S** and **4TS** present very similar CC distances, mostly because of the lack of strain due to their high flexibility, the change from **4S** to **4T** shows lengthening of the double and triple bonds and shortening of the single ones. In fact, the WIs found for the C–C (1.2), C=C (1.7), and C≡C (2.6) bonds in **4S** and **4TS**, in addition with those for **4T** (1.4, 1.4, and 2.3 for single, double, and triple bonds, respectively) confirm the structural data obtained.

In benzene (**5**), sequential substitutions were carried out, leading from **5** to **6**, **7**, **8**, and **9** (one, two, two, and three substitutions, respectively). Compound **6S** shows a bent structure corresponding to a distorted boat. The triplet state, **6T**, corresponds to a planar structure, which lays much higher in energy than the singlet one, so it will not be considered in the present discussion. Compared to benzene (**5S**, 1.395 Å), in **6S** the CC distances change following two different patterns, the C=C bonds decrease (1.354 and 1.346 Å) while the C–C bonds increase (1.492 and 1.428 Å), indicating a loss of the uniform distribution of the electron density, also corroborated with the changes in the WIs from 1.4 in **5** to 1.1, 1.8, and 2.7 (for single, double, and triple bonds, respectively) in **6S**. In **7S** there

is more homogeneity in the C–C and C=C distances than in **6S**, suggesting a partial recovery of the characteristics of the original structure. Similar features can be observed for **8S** with respect to **5S**. In fact, WI for all the CC bonds in both molecules shows more regularity than in **6S**. The case of compound **9** is slightly different than those previously discussed. Thus, while restricted solutions were the most stable for **5**, **6**, **7**, and **8**, the unrestricted singlet open shell structure of **9** (**9U**) was lower in energy than the closed shell (**9S**) or the triplet state (**9T**). The structural differences, in addition to the WIs, are shown in Fig. S1 in Supplementary data. Structure **9U** presents the shortest C=C and C≡C bonds and the longest C–C bonds of the three compounds.

Regarding the bicyclic compounds, transformation of naphthalene (**10**) into **11** involves the substitution of three C–C bonds by three C–C≡C–C groups in the same ring. While the C=C bonds of the expanded ring in compound **11** (1.358 Å, WI=1.7) are 0.016 Å shorter than in the parent ring, the C=C bonds of the six-membered ring are 0.020 Å longer (WI=1.4). The smallest variation is found in the C=C bond, which connects both rings, which suffers a shortening of 0.006 Å with respect to naphthalene. The triple bonds in compound **11** maintain their character as indicated by its WI (2.6).

Transformation of **10** into compounds **12** and **13** involves simultaneous substitution in both rings. The resulting compound **12S** presents an elongation of the C=C bond, which connects both rings (1.540 Å) compared to that of naphthalene (1.431 Å) with a clear reduction of the WI (from 1.2 to 0.9). Additionally, the triple bonds in **12S** show WI closer to double bonds than to triple ones (2.3). However, the most stable solution, **12U**, shows a shorter distance of the same C=C bond (1.418 Å). The C=C distance in **12T** (1.475 Å) is in between of those of **12S** and **12U**. The remaining double bonds in compound **12** measure 1.410, 1.365, and, 1.378 Å for **12S**, **12U**, and **12T**, respectively. The calculated WIs (Fig. S1) show similar behavior than the distances. In addition, triple bonds present same features and variations than single and double bonds, as it can be seen in the bond distances (1.235, 1.217, and 1.224 Å) and in the WIs (2.3, 2.6, and 2.4) for **12S**, **12U**, and, **12T**, respectively. In the case of compound **13**, the C=C bonds present the same distance pattern than in **12**, from the most delocalized to the most localized, **13U**<**13T**<**13S**. Regarding the triple bonds, it is worth to mention than while the central one suffers large variations (WI=2.1, 2.7, and 2.1 for **13S**, **13U**, and **13T**), the other C≡C of the rings maintain almost the same characteristics.

Finally, in azulene (**14**), with the exception of the C–C bond common to both rings, the bond distances range from 1.390 to 1.405 Å. Upon C–C/C–C≡C–C substitution, the resulting compound **15** shows shorter distances in all remaining C=C bonds, varying from 1.361 to 1.382 Å. Additionally, the triple bonds in **15** show WIs, which barely vary (2.5–2.6).

3.1.2. Energy results. In Table 3, the relative energies for all the compounds studied have been summarized. In general, closed shell singlet solutions are the most stable ones, having no instabilities in their wave functions. However, it has been found that in compounds **9**, **12**, and **13**, the open shell solutions were more stable than the closed shell ones and in all those cases, the unrestricted open shell singlet is the most stable. Regarding the relative energies, only those compounds with the same empirical formulae can be compared.

Three compounds (**2**, **3**, and **4**) present ground state boat-like structures and planar transition states, which connect the ground state with their inverted molecule. Thus, we have localized those minima and their transition states, which allow calculating the ring inversion barriers: **2** (8.4 kJ mol^{-1}), **3** (44.1 kJ mol^{-1}), and **4** (6.8 kJ mol^{-1}). Considering that the experimental barrier of COT (**3**)[38] is known to be 53±2 kJ mol^{-1} our calculated value is within acceptable limits. Note that the barrier of **4** (di-dehydro COT) is considerably lower than that of **3**.

Table 3
Relative energies (kJ mol^{-1}) at B3LYP/6-311++G(d,p) for the compounds studied. Only those compounds with the same molecular formula are compared

Compound	E_{rel}	Compound	E_{rel}
1S	—	**9S**	101.5
2S	0.0	**9U**	0.0
2TS	8.4	**9T**	68.4
2T	166.2	**10S**	—
3S	0.0	**11S**	—
3TS	44.1	**12S**	40.55
3T	64.9	**12U**	0.00
4S	0.0	**12T**	23.16
4TS	6.8	**13S**	37.7
4T	83.2	**13U**	0.0
5S	—	**13T**	32.1
6S	—	**14S**	—
7S	—	**15S**	—
8S	—		

As mentioned before, compound **3** ground state is a singlet boat-like structure; the corresponding **3TS** is a planar transition state that lays 44.1 kJ mol^{-1} higher in energy, while the triplet state (**3T**) is found 64 kJ mol^{-1} above the ground state. Comparison of compound **4** with **4TS** and **4T** shows that the difference between ground and transition states is only 6.8 kJ mol^{-1} (six times less than the corresponding **3** to **3TS** transition). Nevertheless, the triplet state (**4T**) remains much higher in energy (76.4 kJ mol^{-1}) than in the case of compound **3**.

The energetic minimum of compound **6** corresponds to a boat-like structure with singlet closed shell state (**6S**). When the triplet state is optimized, the structure became planar with an energy difference of 36.8 kJ mol^{-1} from the singlet one. The ground states of compounds **7** and **8** correspond to singlet closed shells and both compounds present a very high in energy triplet state (more than 200 kJ mol^{-1}). Comparing relative energies, compound **8** is 22.9 kJ mol^{-1} more stable than **7**. It should be noticed that the structure of **8** is not classical in the sense that no Kekulé form can be written, and it only can be represented as a zwitterion or a diradical (Fig. 2).

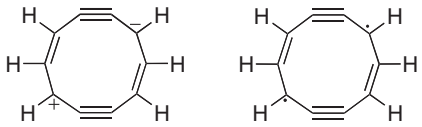

Fig. 2. Possible zwitterionic or diradical structures of **8**.

In the case of compound **9**, the most stable structure corresponds to a single open shell that is −68.4 and −101.5 kJ mol^{-1} more stable than the singlet closed shell and the triplet state, respectively. The fact that the unrestricted solution is the most stable could have dramatic consequences on the aromaticity.

The most stable structure of compound **12** corresponds to an open shell singlet (**12U**), which is −23.2 and −40.5 kJ mol^{-1} more stable than **12T** and **12S**, respectively. Same stability order can be observed for compound **13**, being 32.1 and 37.7 kJ mol^{-1} the relative energies of triplet and closed shell solutions compared to the open shell one.

3.2. NMR properties

3.2.1. NICS results. In order to study the NMR properties of all the compounds considered, we have calculated NICS values at 0, 1, and 2 Å, over the ring center of each molecule. In the case of double

ringed molecules, NICS values were calculated in both rings. To avoid possible interactions with the magnetic field of the atoms, several authors[37,39–43] as well as ourselves[44] recommend to extend the calculations up to 2 Å. Some authors[39,45–47] prefer the use of NICS(*zz*) [also called NICS(out-of-plane)] component to describe (anti)aromaticity. However, the isotropic values are still very much in use, and following our previous experience we have chosen the average NICS instead of the NICS(*zz*) component. NICS values obtained at 0, 1, and 2 Å have been gathered in Tables S2 and S3 for the mono- and bi-cyclic compounds, respectively.

3.2.1.1. Monocyclic compounds. Compound **1** shows large NICS values at 0 and 1 Å due to the proximity of the atom nuclei in the four-membered ring. Compound **2** shows very different NICS values than its parental compound. While in **2** boat-like structure, NICS(0) is very negative, in the **2TS** and **2T** they are positive, the three structures (**S**, **TS**, and **T**) present negative NICS(1) and NICS(2) values, being **S**<**TS**<**T** (Table S2).

Our NICS values for compound **3** are similar to those of Ref. 13 and considering that they were largely discussed in that article. We will not examine them further. In compound **4**, two effects can be analyzed; first, the effect of the C–C substitution (from **3** to **4**) and second the effect of the structural (**S** to **TS**) and singlet or triplet state behavior (**S** to **T**). Comparison between all structures **3** and **4** renders similar trends for **3S** and **4S**, **3TS** and **4TS**, and **3T** and **4T**. Thus, the NICS(0) values of **3** and its derivatives are larger than those of **4**, mainly due to the interaction with the atoms in the ring. In compound **4**, the ring center is located further to any atom nuclei than in **3**, because of the larger ring size. Regarding the change in the structure, **4**, **4TS**, and **4T**, show more similar behavior than in the COT series (**3**). Hence, **4** shows smooth positive NICS values, suggesting non-aromaticity, planar **4TS** presents large positive values, and planar **4T** shows negative NICS (Table S2).

Benzene (**5**) has been extensively studied in the literature (see, for instance, Ref. 13). We have now evaluated the changes of the NICS values upon sequential mono-, bi-, and tri-substitution of C–C by C–C≡C–C. Thus, going from **5** to **6** (mono-substitution) dramatically changes the NICS(0), (1), and (2) from low negative values to medium-large positive ones. This effect is not observed when the double substitution is performed yielding **7** and **8**; in these compounds the NICS values recover its initial negative character, but slightly larger in absolute terms (Table S2).

In compound **9**, and taking into account that the open shell solution is the most stable one, we have studied the changes in the NICS values considering the nature of the wave function. As reported in Table S2, compound **9S** shows much larger and positive NICS values (106.3, 90.9, and 57.6 ppm, for NICS(0), (1), and (2), respectively) than benzene (**5**) and this had been previously reported by Alkorta et al.[14] However, in the present work, when the unrestricted solution (**9U**) is taken into account, the NICS values are significantly smaller (19.6, 16.8, and 10.6 ppm) than the **9S** ones (similar to those reported by Alkorta et al.[14]), but still larger (and positive) than in **5**. Finally, **9T** also presents an NICS pattern (−16.4, −13.2 and −8.7 ppm) similar to that of benzene. These changes in the NICS values when comparing singlet and triplet states were also observed for COT.[13]

3.2.1.2. Bicyclic compounds. The NICS values corresponding to compounds with two rings (**10**–**15**) are presented in Table S3. In all cases, the NICS on each ring were calculated. Naphthalene (**10**) shows similar values than those calculated for benzene. Compound **11** presents two different classes of NICS values, depending on the ring. Thus, in the six-membered ring, the NICS values are negative and larger (in absolute value) than in **10** (ΔNICS=+6.7, +6.3, and +3.0, for NICS(0), (1), and (2), respectively). In the 12-membered ring, there is a change of sign (from negative to positive) and the values are much larger than in **10** (ΔNICS=+19.2, +19.8, and +11.0, for NICS(0), (1), and (2), respectively).

When both rings are symmetrically substituted, the resulting compound **12** presents different features depending on the wave function nature. Structure **12S** shows larger negative values than those found in naphthalene **10S**. However, the NICS values of the open singlet solution, **12U** (the most stable one) are the largest of this family. Finally, the NICS(0), (1), and (2) values of **12T** are in between of those of **12S** and **12U** (Table S3).

If the double ring substitution (C–C by C–C≡C–C) in compound **10** is done asymmetrically (a 12-membered ring and a 14-membered one), the NICS values over the ring center present a more different scenario than in the symmetrical case, despite that the most stable structure for both compounds **12** and **13** corresponds to the singlet unrestricted solution. While in **12** the most negative NICS values corresponds to **12S**, in **13** they correspond to the triplet state, **13T**. The largest NICS values are found in **13S**, while in the symmetrically substituted are found in the singlet open shell structure, **12U** (Table S3).

Finally, compounds **14** and **15** present different NICS(0), (1), and (2) values. While azulene (**14**) shows negative values (aromatic character) in both rings, compound **15** shows positive values in both rings. In the five-membered ring of azulene **14S** the NICS values are very negative, and the values in this small ring in **15** change dramatically (ΔNICS (**15**–**14**)=+23.4, +26.9, and +17.3, for NICS(0), (1), and (2), respectively). However, the changes in the large ring between **14** and **15** are smoother than in the small one (ΔNICS=+10.6, +16.3, and +14.4, for NICS(0), (1), and (2), respectively).

As a good representation of the present discussion on the NICS values of these compounds, we have selected the NICS(1) values as an acceptable compromise between sensitivity and distance from the ring and they are graphically presented in Fig. 3.

Although values as high as −82.2 ppm (in the center of a fullerene with 10 positive charges)[48] and +170.4 ppm (a cyclobutadienyl anion)[49] have been reported, in this series of related neutral carbocycles we have found an extraordinary difference of 109 ppm between the most aromatic, **14S**, and the most antiaromatic, **9S** (Fig. 3).

In addition to the NICS values, a geometrical criterion for the aromaticity has been considered, the harmonic oscillator model of aromaticity (HOMA).[50,51] In Tables S2 and S3 we have reported the HOMA indexes for the carbocyclic systems. In general, while HOMA values describe the aromatic character in agreement with NICS and 3D NICS values for the parent compounds, after the replacement by the C–C≡C–C fragment, the HOMA results differ from the NICS ones. This may be due to the intrinsic definition of the HOMA optimal distance (R_{opt}), which is very dependent on the single and double CC distance bonds. Since the present systems contain several triple bonds, the average CC distance is far from the 1.338 estimated by Krygowski,[36] and thus, HOMA is not adequate to represent the aromatic character of such molecules.

3.2.1.3. NICS isosurfaces. To represent the NICS values in a 3D space, different approaches have been proposed by Sebastiani,[52] Kleinpeter,[18,53–58] Rodriguez-Otero,[59] and Martin[60–65] amongst others. In the present work, we have applied a technique, previously developed in our group,[13,15] which consists in the representation of the NICS values on the 0.001 a.u. electron density isosurface. This isosurface has been shown to resemble the van der Waals one[66] and it can be representative of the reactivity of the molecule. Some authors,[67] have pointed out that at distances far above the ring plane, where the effect of the core electron density and the σ-framework are negligible, the π-electrons are major contributors to the magnetic shielding. Therefore, the 3D representation of the NICS surfaces (resembling van der Waals surfaces)

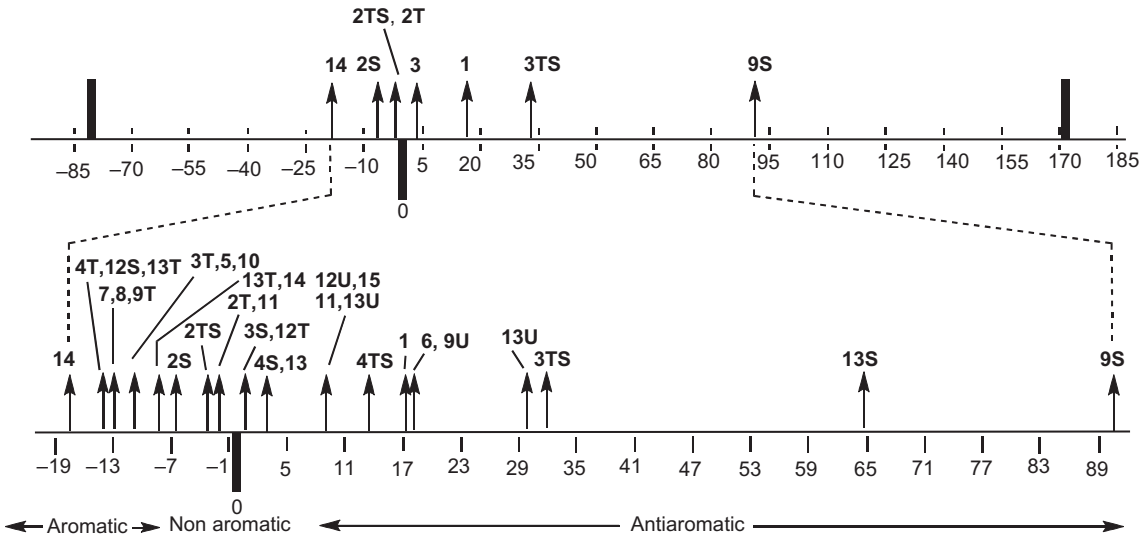

Fig. 3. NICS(1) scale of aromaticity; for an explanation on the extreme values −82.2 and +170.4 ppm (top graph) see the text.

is very convenient since at these distances the core effects are negligible.

This technique allows evaluating the behavior of the NICS, and hence the aromatic features of the molecule, over the three dimensional space. Instead of using a single value along the axis perpendicular to the molecular plane, the NICS isosurfaces provide a large sampling of NICS values, which depend not only of the distance to the center but also take into account the proximity of other atoms. Finally, the minima (or maxima) values obtained on the isosurface provide a quantity in order to compare (not only qualitatively) with a reference (in this case the benzene molecule). The effect that the addition of different bonds and changes in the structure has on the aromaticity can be tracked using this technique.

The NICS isosurfaces for all the compounds studied are represented in Figs. 4, 5, and S2. Negative NICS values are represented in blue (<−4 ppm), green (between −2 and −4 ppm), and yellow (up to 0) areas, while red ones are characteristic of positive NICS values.

The NICS isosurface of compound **1** (Fig. S2, Supplementary data) presents a red area (positive NICS values) over the ring with a maximum value of 4.4 ppm, surrounded by a yellow one and this pattern corresponds to an antiaromatic profile. Compound **2S** shows two different views depending on the position considered. In the convex face (Fig. S2, **2Sa**) two small red areas (0.7 ppm) are found over the outer rings, while in the concave one (Fig. S2, **2Sb**) a single blue-green area (−3.9 ppm) is located over the central ring indicating a small aromatic character. For **2TS** the very negative NICS values area (blue-green) disappears and the maximum value on the surface becomes −1.1 ppm. Finally, when the **2T** is considered, the NICS isosurface becomes yellow-orange (NICS value of −0.8 ppm), indicating lack of aromaticity and resembling those values found in cyclohexane.[13]

The NICS isosurfaces corresponding to all structures in compounds **3** and **4** are depicted in Fig. 4. The isosurfaces of COT (**3**) were previously studied by us;[13] however, even though we will not discuss them here, it is worth mentioning the drastic change in the surface profile when **3S** turns into **3TS** and then into **3T**. In the case of compound **4**, similar NICS isosurface patterns to those found for **3** are observed. The **4S** boat-like structure presents non-aromatic features, similar than those found in the boat-like **3S** and in cyclohexane, but with one difference: the red area over the center of the ring is larger than in **3S**, and the NICS values associated to such a zone (maximum about 2.8 ppm) are slightly larger than in compound **3S** (0.8 ppm). On the contrary, **4TS** (transition state of the inversion of **4S**) shows an NICS pattern very different that the one observed for **4S** (Fig. 4). The large red area (15.0 ppm) situated over the center of the ring and the gradual change of the NICS pattern (into negative values) at the center of the molecular plane, suggests an antiaromatic behavior (similar to that of **3TS**). This result is opposite to what is found in benzene and other aromatic molecules[13] where the negative area is located on the center of the ring and the NICS values become positive along the molecular plane. In the triplet state **4T**, which corresponds to a ground state in the triplet electronic configuration, an aromatic pattern was found similar to that in **3T** and in benzene.

Regarding the benzene series, the NICS isosurface of **5** (Fig. 5) represents the model of aromaticity that can be used for comparison with other molecules, with a blue (negative) area over the center of the ring and a minimum value on the isosurface of −5.8 ppm, changing smoothly into more positive values from the center to the outer part of the molecule, and reaching the most positive values in the molecular plane. The NICS isosurface of **6S** (Fig. 5) with maximum NICS value on the surface of 13.7 ppm, resembles that found for **1S**, suggesting an antiaromatic pattern when one C–C is substituted by a C–C≡C–C fragment. The aromatic character is recovered when the double substitution is performed yielding compounds **7** and **8**, which show minima NICS values of −9.8 and −9.1 ppm, respectively.

The 3D spatial representation of the NICS values of **9S** has also been studied by Kleinpeter and Koch;[18] they found that the values characteristic of the phenyl groups decrease gradually on the macrocycle of dehydro[12]annulene derivatives. Our observations for **9S** reveal that the NICS isosurface presents a large red area (88.8 ppm) in agreement with Kleinpeter's results. However, since we have found that the most stable solution corresponds to the unrestricted **9U**, its NICS isosurface should be more realistic and, in fact, it suggests that dehydro[12]annulene is antiaromatic (in agreement with the data reported by Alkorta[14] and Kleinpeter[18]) showing a maximum NICS value of 15.7 ppm. It is worth to mention that once the triplet state **9T** is taken into account, there is a recovery of the aromatic character of the molecules as observed in its NICS isosurface (−13.2 ppm), which resembles that of benzene.

The 3D NICS representation for naphthalene (**10**) and its derivatives, **11**–**13**, can be found in Fig. S2 (Supplementary data). It can be observed that the **10S** NICS isosurface presents the features found in benzene, i.e., an aromatic pattern with two NICS minima of −6.1 ppm on the surface. When substitution is carried out in only

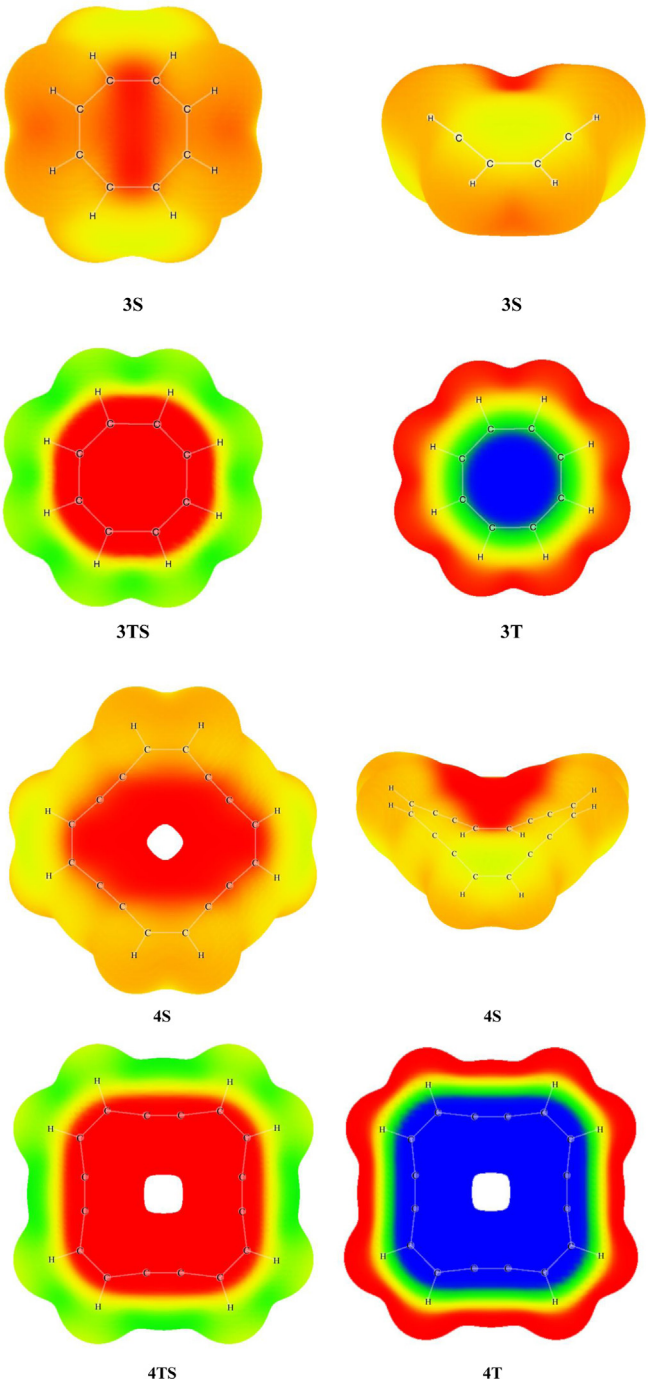

Fig. 4. 3D representation of the NICS values (ppm) on the 0.001 a.u. electron density isosurfaces of compounds **3** and **4**. NICS color scheme: blue <−4.0, green >−4.0, yellow >−2.0, red >0.0.

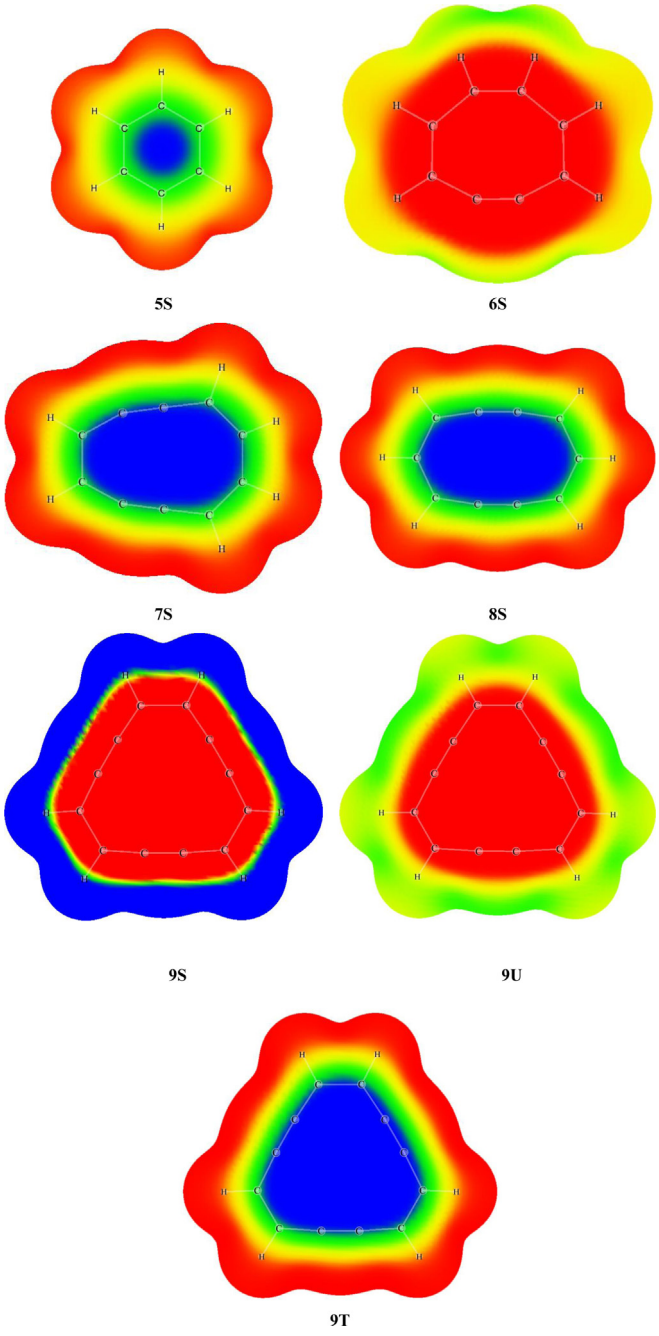

Fig. 5. 3D representation of the NICS values (ppm) on the 0.001 a.u. electron density isosurfaces of benzene and its derivatives. NICS color scheme: blue <−4.0, green >−4.0, yellow >−2.0, red >0.0.

one of the rings, the aromatic character almost disappears, and the resulting isosurface exhibits a large red area in the large cycle with a maximum of 8.7 ppm, and a small green area over the phenyl ring (−2.7 ppm). Thus, the benzene-like pattern found in **10S**, resembles the non-aromatic one in **11**. That was also observed by Kleinpeter,[18] who reported for compound **11S**, a large deshielding isosurface over the large cycle as it was observed in **9S**.

Compound **12S** shows an antiaromatic profile, apparent in the large red (positive) areas over both rings (maximum NICS value of 8.9 ppm), opposite to those found in the naphthalene NICS surface with blue (negative) areas over the rings. Compound **13S** presents similar behavior than **12S**, but the maxima associated to the red areas (27.5 and 9.1 ppm for the small and large ring, respectively) are larger than in the **12S**. Finally, the NICS isosurfaces of compounds **14** and **15**, which are depicted in Fig. S2 (Supplementary data), show that the NICS isosurface of azulene, **14S**, exhibits a large blue area along the molecule, mainly over the two rings (−7.9 and −6.0 ppm for the five- and seven-membered ring, respectively) resembling those found in naphthalene, **10S**. After substituting the C–C bonds by C–C≡C–C fragments in both rings simultaneously (compound **15S**), an important change in aromaticity is observed. As it occurs with compounds **9** and **11**, the blue areas found over the rings associated to negative NICS values change to a red area (positive NICS values), which covers almost the

whole molecule showing two maxima of 10.0 and 8.4 ppm that correspond to the antiaromatic character of **15S**.

3.2.1.4. NMR chemical shifts. Although chemical shifts have a complex relationship with aromaticity (and for this reason, Schleyer introduced the NICS, see before),[68–70] they have the advantage to be an observable. We have calculated the absolute NMR shieldings (σ, ppm) and transformed them into chemical shifts (δ, ppm) by means of empirical relationships established for ^{1}H and ^{13}C,[71,72] and the results are presented in Table 4.

These chemical shifts (Table 4) follow the same trends as the NICS an indication that they also are sensitive to aromaticity/non-aromaticity/antiaromaticity criteria. Besides when compared with the available experimental chemical shifts they show very good agreement.

The chemical shifts, presented in Table 4, follow the same trends as the NICS an indication that they also are sensitive to aromaticity/non-aromaticity/antiaromaticity criteria. Besides when compared with the available experimental chemical shifts they show very good agreement.

Table 4
^{1}H and ^{13}C NMR absolute shielding and chemical shifts (both in ppm)

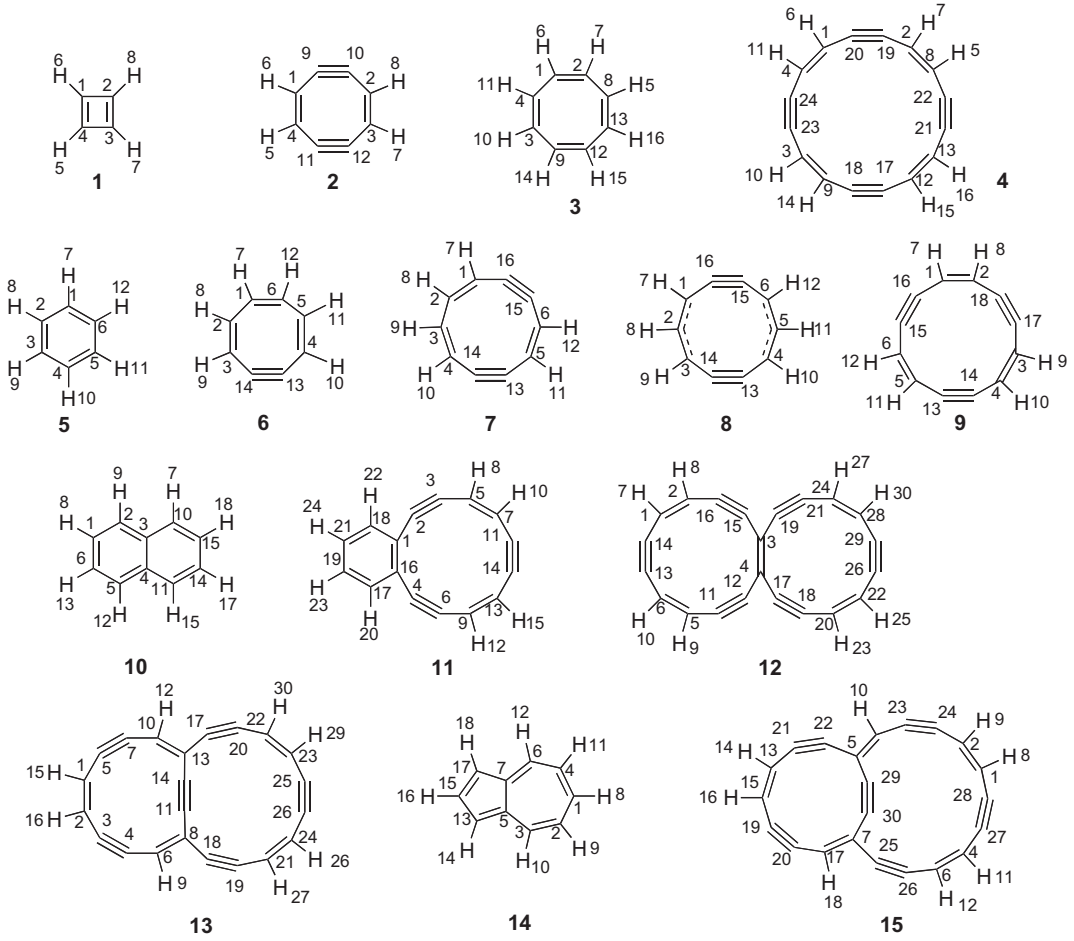

	Atom	δ Calcd	δ Exp.
1S	1C	140.2	145±10[a]
	5H	5.7	5.76[73]
2S	1C	127.8	
	9C	173.0	
	5H	6.4	
2TS	1C	142.6	
	9C	160.1	
	5H	7.0	
2T	1C	121.3	
	9C	174.9	
	5H	6.2	
3S	1C	135.8	131.5[74]
	5H	5.8	5.78[75]
3TS	1C	134.6	
	5H	1.4	
3T	1C	121.7	
	5H	7.8	
4S	1C	122.8	
	17C	104.7	
	5H	5.4	

Table 4 (*continued*)

	Atom	δ Calcd	δ Exp.
4TS	1C	123.1	
	17C	105.4	
	5H	2.5	
4T	1C	108.9	
	17C	129.0	
	5H	10.3	
5S	1C	127.8	128.5[74]
	7H	7.4	7.27[77]
6S	1C	137.9	
	2C	152.1	
	3C	119.8	
	13C	121.1	
	7H	3.4	
	8H	4.1	
	9H	3.2	
7S	1C	106.6	
	2C	131.2	
	5C	121.1	
	13C	123.7	
	14C	129.8	
	7H	8.0	
	8H	8.2	
	11H	8.0	
8S	1C	106.4	
	2C	138.2	
	13C	129.2	
	7H	7.9	
	8H	8.6	
9S	1C	131.4	
	13C	223.5	
	7H	−12.2	4.42[14]
9U	1C	128.1	
	13C	104.6	
	7H	2.7	4.42[14]
9T	1C	109.6	
	13C	135.2	
	7H	8.7	4.42[14]
10S	1C	125.4	125.6[74]
	2C	126.7	127.7[74]
	3C	134.6	133.3[74]
	7H	7.8	7.73[73]
	8H	7.5	7.38[73]
11S	1C	132.2	
	2C	104.8	
	3C	97.6	
	5C	125.6	
	7C	124.2	
	11C	104.3	
	17C	133.0	
	19C	128.8	
	8H	4.2	
	10H	4.2	
	20H	5.9	
	23H	6.2	
12S	1C	111.5	
	2C	112.4	
	3C	84.3	
	11C	129.2	
	12C	139.8	
	13C	135.8	
	5C	140.1	
	8H	9.4	
12U	1C	123.5	
	2C	124.2	
	3C	121.9	
	11C	111.6	
	12C	109.2	
	13C	109.1	
	7H	3.9	
	8H	3.9	
12T	1C	119.4	
	2C	121.3	
	3C	107.3	
	11C	122.0	
	12C	123.1	
	13C	115.8	

(*continued on next page*)

Table 4 (*continued*)

	Atom	δ Calcd	δ Exp.
	7H	5.7	
	8H	5.9	
13S	1C	127.3	
	3C	206.9	
	4C	204.7	
	6C	126.1	
	8C	125.2	
	11C	172.2	
	17C	126.2	
	19C	127.2	
	21C	115.7	
	23C	119.4	
	25C	132.8	
	9H	−7.5	
	15H	−7.4	
	26H	2.9	
	27H	2.4	
13U	1C	131.8	
	2C	131.8	
	3C	118.0	
	4C	112.4	
	6C	129.8	
	8C	132.6	
	11C	114.1	
	17C	102.0	
	19C	103.4	
	21C	120.7	
	23C	124.6	
	25C	105.9	
	9H	−1.0	
	15H	−0.5	
	27H	2.6	
	26H	2.9	
13T	1C	111.7	
	3C	133.2	
	4C	130.3	
	6C	111.0	
	8C	106.1	
	11C	106.9	
	17C	117.3	
	19C	110.5	
	21C	113.5	
	23C	116.6	
	25C	109.4	
	9H	10.4	
	15H	9.7	
	26H	9.0	
	27H	9.2	
14S	1C	137.5	136.9[74]
	2C	121.2	122.6[74]
	3C	135.9	136.4[74]
	5C	140.1	140.1[74]
	13C	116.8	118.1[74]
	15C	137.7	136.9[74]
	8H	7.7	7.61[76]
	9H	7.2	7.19[76]
	10H	8.4	8.37[76]
	14H	7.0	7.42[76]
	16H	7.9	7.93[76]
15S	1C	118.3	
	2C	123.6	
	3C	108.9	
	4C	128.1	
	5C	129.5	
	6C	119.4	
	7C	131.2	
	13C	124.1	
	15C	130.9	
	17C	122.1	
	19C	114.7	
	20C	112.8	
	21C	111.6	
	22C	113.9	
	23C	109.8	
	24C	108.0	
	25C	104.4	
	26C	104.3	

Table 4 (*continued*)

Atom	δ Calcd	δ Exp.
27C	105.2	
28C	109.7	
29C	119.7	
30C	120.0	
8H	3.4	
9H	3.4	
10H	2.4	
11H	3.7	
12H	3.3	
14H	3.5	
16H	3.9	
18H	3.0	

[a] This value was provided by Professor Facelli (personal communication) based on their work from Ref. 78.

4. Conclusions

The most stable minima for all the compounds studied have been considered. It has found no instabilities in their wave functions. The relative energies of those compounds with same molecular formula vary from 6.8 to 166.2 kJ mol^{-1}.

While upon substitution of the C–C bonds by C–C≡C–C in cyclobutadiene the C=C remaining bonds suffer an elongation, in the COT and benzene derivatives a shortening occurs. Bicyclic compounds present diverse behaviors depending on the mono- or simultaneous di-substitution of one or both rings.

NICS calculated at 0, 1, and 2 Å as well as 3D NICS representations reveal that while in cyclobutadiene, benzene, naphthalene, and azulene, there is a change in the aromatic or antiaromatic character of the molecule upon substitution, in the case of COT the NICS patterns and, hence, the aromatic behaviors are maintained.

Upon substitution in compound **1** (antiaromatic), compound **2** resulted in different states: **2S** (aromatic) and **2T** (non-aromatic). From compound **3S** (non-aromatic) to **4S** (non-aromatic) the aromatic character remains, as it happens with their different states **3TS** (antiaromatic) to **4TS** (antiaromatic), and **3T** (aromatic) to **4T** (aromatic). Benzene, **5** (aromatic), changes into **6** (antiaromatic) with a single replacement, while two simultaneous incorporations of the C–C≡C–C fragment, lead to **7** and **8** (both aromatic). Compound **9** shows different behaviors, depending on the state considered, **9U** (antiaromatic) and **9T** (aromatic). Both bicyclic compounds, naphthalene **10** (aromatic) and azulene **14** (aromatic), suffer a change in their aromatic character upon substitution, leading to antiaromatic compounds in all the cases, **11**, **12**, **13**, and **15**.

Finally, the calculated ^{1}H and ^{13}C NMR chemical shifts are qualitatively consistent with the picture obtained from the NICS analysis reproducing well the experimental data.

Acknowledgements

We thank the Ministerio de Ciencia e Innovación (project no. CTQ2012-13129-C02-02) and the Comunidad Autónoma de Madrid (project MADRISOLAR2, ref. S2009/PPQ-1533) for continuous support. Thanks are given to the CTI (CSIC) and the Centro de Computación Científica de la Universidad Autónoma de Madrid for allocation of computing time. Prof. Julio C. Facelli (University of Utah) assistance is greatly acknowledged.

Supplementary data

Coordinates, Wiberg indexes, HOMA indexes, absolute energies (a.u.), NMR absolute chemical shifts, and 3D NICS isosurfaces at the B3LYP/6-311++G** level of theory of all studied compounds. Supplementary data associated with this article can be found in the online version, at http://dx.doi.org/10.1016/j.tet.2013.06.072.

References and notes

1. Zubarev, D. Y.; Frenklach, M.; Lester, W. A., Jr. *Phys. Chem. Chem. Phys.* **2012**, *14*, 12075.
2. Martín-Martínez, F. J.; Fias, S.; Van Lier, G.; De Proft, F.; Geerlings, P. *Chem.—Eur. J.* **2012**, *18*, 6183.
3. Gellini, C.; Salvi, P. R. *Symmetry* **2010**, *2*, 1846.
4. Badger, G. M. *Aromatic Character and Aromaticity*; Cambridge University Press: London, UK, 1969.
5. Symposium on Aromaticity, S. E. *Aromaticity: An International Symposium Held at Sheffield on 6th–8th July 1966; Organized Jointly by the University of Sheffield and the Chemical Society*; Chemical Society: London, 1967.
6. Minkin, V. I.; Glukhovtsev, M. N.; Simkin, B. Y. *Aromaticity and Antiaromaticity. Electronic and Structural Aspects*; Wiley-Interscience: New York, NY, 1994.
7. Nishinaga, T.; Ohmae, T.; Aita, K.; Takase, M.; Iyoda, M.; Arai, T.; Kunugi, Y. *Chem. Commun.* **2013**, 5354.
8. Baughman, R. H.; Eckhardt, H.; Kertesz, M. *J. Chem. Phys.* **1987**, *87*, 6687.
9. Jiao, Y.; Du, A.; Hankel, M.; Zhu, Z.; Rudolph, V.; Smith, S. C. *Chem. Commun.* **2011**, 11843.
10. Cui, H.-J.; Sheng, X.-L.; Yan, Q.-B.; Zheng, Q.-R.; Su, G. *Phys. Chem. Chem. Phys.* **2013**, *15*, 8179.
11. Karadakov, P. B. *J. Phys. Chem. A* **2008**, *112*, 7303.
12. Henrik, H. O. *Nat. Chem.* **2012**, *4*, 969.
13. Sánchez-Sanz, G.; Alkorta, I.; Trujillo, C.; Elguero, J. *Tetrahedron* **2012**, *68*, 6548.
14. Alkorta, I.; Rozas, I.; Elguero, J. *Tetrahedron* **2001**, *57*, 6043.
15. Alkorta, I.; Sánchez-Sanz, G.; Trujillo, C.; Elguero, J.; Claramunt, R. M. *Arkivoc* **2012**, *ii*, 85.
16. Kelly, B.; Sánchez-Sanz, G.; Blanco, F.; Rozas, I. *Comput. Theor. Chem.* **2012**, *998*, 64.
17. Inoue, K.; Takeuchi, H.; Konaka, S. *J. Phys. Chem. A* **2001**, *105*, 6711.
18. Kleinpeter, E.; Koch, A. *Tetrahedron* **2013**, *69*, 1481.
19. Macaluso, M.; Parish, C. A.; Hoffmann, R.; Scott, L. T. *J. Org. Chem.* **2004**, *69*, 8093.
20. Oth, J. F. M. *Pure Appl. Chem.* **1971**, *25*, 573.
21. Yavari, I.; Norouzi-Arasi, H. *J. Mol. Struct.: THEOCHEM* **2002**, *593*, 199.
22. Karadakov, P. B. *J. Phys. Chem. A* **2008**, *112*, 12707.
23. Hege, H.-C.; Manz, J.; Marquardt, F.; Paulus, B.; Schild, A. *Chem. Phys.* **2010**, *376*, 46.
24. Wu, J. I.; Fernández, I.; Mo, Y.; Schleyer, P. v. R. *J. Chem. Theor. Comput.* **2012**, *8*, 1280.
25. Becke, A. D. *J. Chem. Phys.* **1993**, *98*, 5648.
26. Lee, C. T.; Yang, W. T.; Parr, R. G. *Phys. Rev. B* **1988**, *37*, 785.
27. Frisch, M. J.; Pople, J. A.; Binkley, J. S. *J. Chem. Phys.* **1984**, *80*, 3265.
28. Schleyer, P. v. R.; Maerker, C.; Dransfeld, A.; Jiao, H.; Hommes, N. J. R. v. E. *J. Am. Chem. Soc.* **1996**, *118*, 6317.
29. London, F. *J. Phys. Radium* **1937**, *8*, 397.
30. Ditchfield, R. *Mol. Phys.* **1974**, *27*, 789.
31. Bulat, F.; Toro-Labbé, A.; Brinck, T.; Murray, J.; Politzer, P. *J. Mol. Model.* **2010**, *16*, 1679.
32. Frisch, M. J.; Trucks, G. W.; Schlegel, H. B.; Scuseria, G. E.; Robb, M. A.; Cheeseman, J. R.; Scalmani, G.; Barone, V.; Mennucci, B.; Petersson, G. A.; Nakatsuji, H.; Caricato, M.; Li, X.; Hratchian, H. P.; Izmaylov, A. F.; Bloino, J.; Zheng, G.; Sonnenberg, J. L.; Hada, M.; Ehara, M.; Toyota, K.; Fukuda, R.; Hasegawa, J.; Ishida, M.; Nakajima, T.; Honda, Y.; Kitao, O.; Nakai, H.; Vreven, T.; Montgomery, J. J. A.; Peralta, J. E.; Ogliaro, F.; Bearpark, M.; Heyd, J. J.; Brothers, E.; Kudin, K. N.; Staroverov, V. N.; Kobayashi, R.; Normand, J.; Raghavachari, K.; Rendell, A.; Burant, J. C.; Iyengar, S. S.; Tomasi, J.; Cossi, M.; Rega, N.; Millam, N. J.; Klene, M.; Knox, J. E.; Cross, J. B.; Bakken, V.; Adamo, C.; Jaramillo, J.; Gomperts, R.; Stratmann, R. E.; Yazyev, O.; Austin, A. J.; Cammi, R.; Pomelli, C.; Ochterski, J. W.; Martin, R. L.; Morokuma, K.; Zakrzewski, V. G.; Voth, G. A.; Salvador, P.;

Dannenberg, J. J.; Dapprich, S.; Daniels, A. D.; Farkas, Ö.; Foresman, J. B.; Ortiz, J. V.; Cioslowski, J.; Fox, D. J. Gaussian: Wallingford, CT, 2009.
33. Reed, A. E.; Curtiss, L. A.; Weinhold, F. *Chem. Rev.* **1988**, *88*, 899.
34. Glendening, E. D.; Weinhold, F. *J. Comput. Chem.* **1998**, *19*, 593.
35. Glendening, E. D.; Badenhoop, J. K.; Weinhold, F. *J. Comput. Chem.* **1998**, *19*, 628.
36. Kruszewski, J.; Krygowski, T. M. *Tetrahedron Lett.* **1972**, *13*, 3839.
37. Szwacki, N.; Weber, V.; Tymczak, C. *Nanoscale Res. Lett.* **2009**, *4*, 1085.
38. Kato, S.; Lee, H. S.; Gareyev, R.; Wenthold, P. G.; Lineberger, W. C.; DePuy, C. H.; Bierbaum, V. M. *J. Am. Chem. Soc.* **1997**, *119*, 7863.
39. Stanger, A. *J. Org. Chem.* **2006**, *71*, 883.
40. Ghiasi, R. *J. Mol. Struct.: THEOCHEM* **2008**, *853*, 77.
41. Kassaee, M. Z.; Ghambarian, M.; Musavi, S. M. *Heteroat. Chem.* **2008**, *19*, 377.
42. Tsipis, C. A. *Coord. Chem. Rev.* **2005**, *249*, 2740.
43. Winkler, M.; Cakir, B.; Sander, W. *J. Am. Chem. Soc.* **2004**, *126*, 6135.
44. Alkorta, I.; Azofra, L.; Sánchez-Sanz, G.; Elguero, J. *Struct. Chem.* **2012**, *23*, 1245.
45. Solà, M.; Feixas, F.; Jiménez-Halla, J. O. C.; Matito, E.; Poater, J. *Symmetry* **2010**, *2*, 1156.
46. von Ragué Schleyer, P.; Manoharan, M.; Wang, Z.-X.; Kiran, B.; Jiao, H.; Puchta, R.; van Eikema Hommes, N. J. R. *Org. Lett.* **2001**, *3*, 2465.
47. Baranac-Stojanović, M.; Koch, A.; Kleinpeter, E. *Chem.—Eur. J.* **2012**, *18*, 370.
48. Aihara, J.-i.; Tamaribuchi, T. *Chem. Phys. Lett.* **2003**, *374*, 104.
49. Tsipis, A. C. *Phys. Chem. Chem. Phys.* **2009**, *11*, 8244.
50. Krygowski, T. M.; Cyrański, M. K. *Chem. Rev.* **2001**, *101*, 1385.
51. Zborowski, K.; Alkorta, I.; Elguero, J.; Proniewicz, L. *Struct. Chem.* **2013**, *24*, 543.
52. Sebastiani, D.; Parker, M. *Symmetry* **2009**, *1*, 226.
53. Kleinpeter, E.; Bölke, U.; Koch, A. *J. Phys. Chem. A* **2010**, *114*, 7616.
54. Kleinpeter, E.; Klod, S.; Koch, A. *J. Mol. Struct.: THEOCHEM* **2007**, *811*, 45.
55. Kleinpeter, E.; Koch, A. *Tetrahedron* **2009**, *65*, 5350.
56. Kleinpeter, E.; Koch, A.; Shainyan, B. A. *J. Mol. Struct.: THEOCHEM* **2008**, *863*, 117.
57. Kleinpeter, E.; Lammermann, A.; Kuhn, H. *Org. Biomol. Chem.* **2011**, *9*, 1098.
58. Klod, S.; Kleinpeter, E. *J. Chem. Soc., Perkin Trans. 2* **2001**, 1893.
59. Montero-Campillo, M.; Rodríguez-Otero, J.; Cabaleiro-Lago, E. *J. Mol. Model.* **2007**, *13*, 919.
60. Martin, N. H.; Floyd, R. M.; Woodcock, H. L.; Huffman, S.; Lee, C.-K. *J. Mol. Graph. Model.* **2008**, *26*, 1125.
61. Martin, N. H.; Loveless, D. M.; Main, K. L.; Wade, D. C. *J. Mol. Graph. Model.* **2006**, *25*, 389.
62. Martin, N. H.; Nance, K. H. *J. Mol. Graph. Model.* **2002**, *21*, 51.
63. Martin, N. H.; Rowe, J. E.; Pittman, E. L. *J. Mol. Graph. Model.* **2009**, *27*, 853.
64. Martin, N. H.; Rowe, J. E.; Pittman, E. L. *J. Mol. Graph. Model.* **2010**, *28*, 650.
65. Martin, N. H.; Teague, M. R.; Mills, K. H. *Symmetry* **2010**, *2*, 418.
66. Bader, R. F. W.; Carroll, M. T.; Cheeseman, J. R.; Chang, C. *J. Am. Chem. Soc.* **1987**, *109*, 7968.
67. Foroutan-Nejad, C.; Shahbazian, S.; Rashidi-Ranjbar, P. *Phys. Chem. Chem. Phys.* **2010**, *12*, 12630.
68. Karplus, M.; Pople, J. A. *J. Chem. Phys.* **1963**, *38*, 2803.
69. Schleyer, P. v. R.; Jiao, H. *Pure Appl. Chem.* **1996**, *68*, 209.
70. Liu, L. V.; Tian, W. Q.; Chen, Y. K.; Zhang, Y. A.; Wang, Y. A. *Nanoscale* **2010**, *2*, 254.
71. Silva, A. M. S.; Sousa, R. M. S.; Jimeno, M. L.; Blanco, F.; Alkorta, I.; Elguero, J. *Magn. Reson. Chem.* **2008**, *46*, 859.
72. Blanco, F.; Alkorta, I.; Elguero, J. *Magn. Reson. Chem.* **2007**, *45*, 797.
73. Wannere, C. S.; Schleyer, P. v. R. *Org. Lett.* **2003**, *5*, 605.
74. Kalinowski, H. O.; Berger, S.; Braun, S. *Carbon-13 NMR Spectroscopy*; John Wiley & Sons: Chichester, UK, 1988.
75. McMurray, J. E. *Organic Chemistry*, 8th ed.; Brook/Cole: Pacific Grove, CA, 2012.
76. Rogoski, J. M.; Nagornyy, P. http://www.geocities.ws/justin_m_r/papers/azulene.
77. Jackman, L. M. *Applications of Nuclear Magnetic Resonance Spectroscopy in Organic Chemistry*; Pergamon: London, UK, 1962.
78. Orendt, A. M.; Arnold, B. R.; Radziszewski, J. G.; Facelli, J. C.; Malsch, K. D.; Strub, H.; Grant, D. M.; Michl, J. *J. Am. Chem. Soc.* **1988**, *110*, 2648.